Resonant x-ray scattering study of magnetic ordering due to Fermi-surface nesting in $SmNi_2Ge_2$

Zahirul Islam,[1,2,*] J. C. Lang,[2] L. Vasiliu-Doloc,[1,2] G. Srajer,[2] and P. C. Canfield[3]
[1]*Department of Physics, Northern Illinois University, DeKalb, Illinois 60115*
[2]*Advanced Photon Source, Argonne National Laboratory, Argonne, Illinois 60439*
[3]*Ames Laboratory and Department of Physics and Astronomy, Iowa State University, Ames, Iowa 50011*
(Received 19 October 2000; revised manuscript received 19 July 2001; published 27 December 2001)

We report the results of x-ray resonant scattering studies of samarium nickel germanide ($SmNi_2Ge_2$) compound. We confirm that the magnetic structures of this material are in accordance with Fermi-surface nesting as was hypothesized earlier. $SmNi_2Ge_2$ orders in an *incommensurate* antiferromagnetic (AF) structure characterized by a single propagation vector $\mathbf{q}=(0,0,q_z)$. The value of q_z is temperature dependent and approaches ~ 0.775 r.l.u. near $T_N=17.7$ K. Below $T_t=11.8$ K, the AF structure is characterized by $q_z=0.79\pm0.002$, indicating a long-period-ordered phase. Ordered moments are confined to the basal plane in both the phases, as evidenced by the **Q** dependence of the magnetic-peak intensities. The temperature dependence of the magnetic structures is consistent with the ''superzone'' gap theory. In addition, a strong quadrupolar resonance below the Sm L_{III} edge was observed and compared to recent theoretical work.

DOI: 10.1103/PhysRevB.65.054404 PACS number(s): 75.25.+z, 75.10.−b, 75.30.−m, 78.70.Ck

I. INTRODUCTION

Materials with complex crystal structure and multiatom composition, such as the ternary and quaternary rare-earth intermetallics, possess intricate electronic structures. One then expects rather complicated and competing interactions to be at play in determining their magnetic ground state.[1,2] Nevertheless, in some cases it is possible to describe the magnetic behavior, which is determined primarily by the open but localized and correlated $4f$ shell, of a whole family of materials rather well, on the basis of a simple Hamiltonian containing crystal electric field (CEF) and Heisenberg-type exchange interactions alone. Whereas the CEF effects are single-ion phenomena that create a semiclassical potential to restrict the direction of the $4f$ moment at a particular site, the latter, formally known as the RKKY-type exchange interaction, plays the prominent role in establishing magnetic long-range order.[3–5] The rare-earth (R) nickel germanides $R\mathrm{Ni}_2\mathrm{Ge}_2$,[6] with the well-studied $\mathrm{ThCr}_2\mathrm{Si}_2$-type structure appear to be such systems. Although the detailed nature of the ground state in these materials is determined by a subtle balance between RKKY and CEF interactions, very close to the transition the RKKY term can be dominant because it varies as σ^2 (where $\sigma=|\langle\mathbf{J}\rangle|/J$ is the thermally averaged reduced moment) compared to the $\sigma^{l(l+1)/2}$ dependence (Zener power law) of the lth-order CEF term (see Ref. 7 and references therein). Since the exchange energy due to the RKKY interaction is proportional to the negative of the generalized electronic susceptibility $\chi_0(\mathbf{q})$,[3,5,8] the stable magnetic structure at the onset of ordering corresponds to the one with a $\mathbf{q}$ that maximizes $\chi_0(\mathbf{q})$. If nesting between various parts of the Fermi surface exists for a particular wave vector $\mathbf{q}_{\mathrm{nest}}$, the nature of the RKKY interaction is dramatically influenced (see Roth *et al.*)[9] and $\chi_0(\mathbf{q})$ becomes sharply peaked at $\mathbf{q}_{\mathrm{nest}}$, which determines the magnetic wave vector that characterizes the ordered state. In a recent study,[10] $\chi_0(\mathbf{q})$ calculations were carried out using the tight-binding linear-muffin-tin-orbital electronic bands within the atomic sphere approximation, in order to correlate electronic structures to magnetic order in the $R\mathrm{Ni}_2\mathrm{Ge}_2$ series.

According to that work, there exists pronounced nesting between two bands with strong $5d$ character at the Fermi level in these materials that is responsible for the single *incommensurate*, magnetic modulation vector of the form $\mathbf{q}=(0,0,q_z)$, with q_z in the range 0.75–0.81 r.l.u., observed in the tripositive R members of the series. Based upon the nesting picture and the observation of CEF anisotropy, the magnetic ground state of the samarium nickel germanide ($SmNi_2Ge_2$) compound has been hypothesized to be a basal-plane helical structure just below the Néel transition.[11] To our knowledge, no definitive work on its magnetic structures exists. However, bulk characterization via susceptibility and magnetization measurements on single crystals (see below) has been published earlier (see Ref. 12). The primary objective of this work is to investigate the hypothesis about the magnetic structures of the Sm member of the series using the x-ray resonant exchange scattering (XRES) technique.[13,14]

X-ray magnetic scattering is a powerful tool for the study of magnetism in condensed matter (see Refs. 15 and 16 and references therein). Intrinsic high-**Q** resolution, ability to separate spin and orbital moments, resonant enhancement of the cross section, elemental selectivity as well as orbital specificity, and indifference to neutron-opaque elements (such as Sm) make this technique indispensable and often superior to the conventional magnetic neutron-diffraction methods. For this work we employed the XRES (Refs. 13 and 14) technique to take advantage of its resonant enhancement, particularly well suited for the study of high-quality, small single crystals of materials containing small magnetic moments.

Purely from the XRES point of view, Sm is particularly interesting, since only a few materials containing Sm have been studied thus far. This is primarily due to the fact that single crystals of Sm-containing compounds are harder to

grow compared to those with some other R elements. In a previous study on $SmNi_2B_2C$ compounds by Detlefs and co-workers,[17] both quadrupolar and dipolar resonances have been observed at the Sm L_{III} edge. The **Q** dependence of the relative weight between these resonances found use in refining the direction of the ordered moments within the fourfold-degenerate tetragonal basal plane. Furthermore, a recent study[18] on a 5000-Å epitaxial thin film of elemental Sm grown on sapphire showed two strong resonance features above both the L_{II} and L_{III} edges, as well as a strong resonance below the L_{III} edge. Such observations of multiple resonances above an edge cannot be readily explained within the framework of current theoretical models based on an atomic description of the resonance processes. Further investigations on Sm-containing materials with different electronic structures can be useful in revealing systematics in the resonance phenomena.

High-quality single crystals of the entire RNi_2Ge_2 series (except the Pm member) have been grown by a high-temperature solution-growth technique.[19] Crystals of these materials have metallic luster and platelike morphology, with the larger flat facets perpendicular to the tetragonal $\hat{\mathbf{c}}$ axis. According to x-ray-diffraction characterization, these crystals are of high quality and free of any detectable level of impurity phases other than the surface flux. Transport, magnetization, and specific heat measurements performed on single crystals of these compounds were published in Ref. 12. Here we summarize the results on the Sm member of the family pertinent to our current study. The temperature dependence of the low-field susceptibilities $\chi_{\parallel}$ ($\mathbf{H}\parallel\hat{\mathbf{c}}$) and $\chi_{\perp}$ ($\mathbf{H}\perp\hat{\mathbf{c}}$) were found to be anisotropic below 100 K, with $\chi_{\perp} > \chi_{\parallel}$. The transition from paramagnetic to an antiferromagnetic (AF) phase occurs at T_N of 17.9 K. As the temperature is lowered through T_N, $\chi_{\parallel}$ continues to increase, while $\chi_{\perp}$ decreases, suggesting an easy plane of magnetization in this compound. This behavior is in contrast to that in an uniaxial system, such as $TbNi_2Ge_2$,[12] where the anisotropy is reversed. Two additional transitions at lower temperatures below T_N are also observed, at $T_t = 11.8$ K and $T_{t'} = 5.5$ K, respectively. However, the latter one is only prominent in the $\chi_{\parallel}(T)$ measurements. Due to the minimum obtainable temperature of 8.0 K, in this work we are primarily concerned with the ordered phases above $T_{t'}$.

The outline of the paper is as follows. In Sec. II we summarize the experimental setup. Next, we present XRES results in detail (Sec. III), including the resonance properties and the polarization analysis (Sec. III A), the temperature evolution of the magnetic phases, and the **Q** dependence of the integrated intensities (Secs. III B and III C, respectively), followed by concluding remarks (Sec. IV).

II. EXPERIMENTAL DETAILS

The XRES studies were performed on the 1-BM bending-magnet beamline at the Advanced Photon Source (APS) located in Argonne National Laboratory.[20] The primary optical components of this beamline are two cylindrically bent mirrors and a double-crystal monochromator (DCM). A palladium-coated cylindrical mirror is located before the DCM in order to vertically collimate the beam, thereby improving the energy resolution. In this work a Si (111) crystal was used to monochromatize the beam providing an energy resolution of ~1.5 eV for incident energy around 7 keV.[20] The second crystal in the DCM is sagittally bent, which focuses the beam horizontally into the experimental end station. Energy scans spanning ~50 eV through the Sm L_{II} and L_{III} edges were carried out by rocking the crystals in unison, while keeping the translation of the second crystal fixed. Another palladium-coated cylindrical mirror was located after the DCM to allow for vertical focusing of the beam. For this experiment, a third mirror was placed inside the experimental station prior to the Huber goniometer to provide additional harmonic suppression, thereby ensuring a clean monochromatic beam incident on the sample. The incident monochromatic beam was focused both vertically and horizontally, delivering $\sim 10^{12}$ photons/sec at 100 mA in a spot size of 600 μm$\times$700 μm, respectively, at the sample.

For this experiment a rectangular sample with dimensions $2.5\times0.9\times0.3\,\mathrm{mm}^3$ was aligned with the $[H,0,L]$ zone in the vertical scattering plane. The width of the sample was chosen to ensure that the beam completely bathes the crystal in the scattering plane at all angles of interest. The sample was oriented, cut, and polished perpendicular to [0,0,1], to eliminate residual flux on the as-grown surface and increase reflectivity. The mosaic at (0,0,4) was ~0.05°. Initially, the incident photon energy was tuned to the L_{II} edge (7.312 keV) of Sm in order to use resonant enhancement.[14,13] The (0,0,6) reflection from a flat pyrolytic graphite crystal was used as the polarization analyzer. For measurements of the integrated intensity, the analyzer was removed and a Ge solid-state detector (SSD) was used to collect both the diffracted beam and the fluorescence from the sample. However, the energy resolution (~ 150 eV) of the SSD was not sufficient to allow for a complete discrimination of the L_{β} fluorescence from the elastic channel. The sample was sealed in a Be can with He exchange gas and cooled in a closed-cycle He refrigerator with a base temperature of 8.0 K. In this setup the raw intensity for the $(0,0,4)^+$ first-order magnetic satellite peak was ~2600 counts/sec above background at the L_{II} edge for the dipolar resonance at 8.0 K. All temperature-dependent measurements were carried out by warming the sample from lower to higher temperature.

III. RESULTS

A. Resonance and polarization properties

From previous studies of RNi_2Ge_2 compounds, the magnetic modulation vector was expected to lie along the Λ line $[0,0,L]$ in the Brillouin zone (BZ), with a q_z value in the range mentioned above. Figure 1 shows the reciprocal lattice scan, at 8.0 K, along $[0,0,L]$ as the incident photon energy (E_i) was varied across the Sm L_{II} edge. As E_i was gradually changed from 7.285 to 7.385 keV, a sharp peak emerged in the $[0,0,L]$ scan near $\mathbf{q}=(0,0,0.79)$, reaching a maximum for $E_i = 7.314$ keV. Upon further increasing the energy, the intensity of the peak decreased, eventually reducing to the background at 7.325 keV. The intensity of the peak reduced

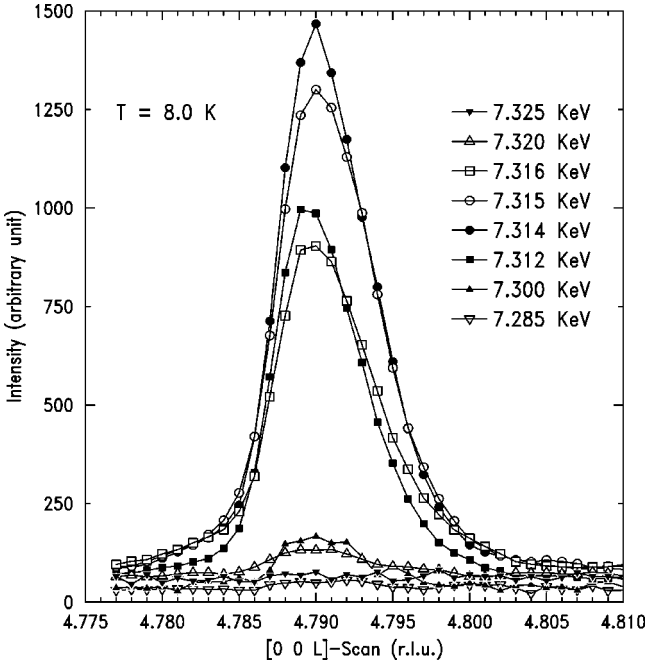

FIG. 1. $[0,0,L]$ scans showing the emergence and diminishment of the superlattice reflection as the incident photon energy is varied through the resonance.

by some 50% as E_i was only 2–3 eV away from 7.314 keV, indicating sharpness of the resonance in energy.

With E_i fixed at 7.314 keV, we performed a careful scan across the BZ along the Λ line, as shown in Fig. 2. Two fundamental superlattice peaks associated with the (0,0,4) and (0,0,6) charge peaks, marked $(0,0,4)^+$ and $(0,0,6)^-$, respectively, appeared symmetrically on either side of the BZ boundary. In addition, two peaks, weak and resolution limited, corresponding to the second harmonic $2\mathbf{q}$, were observed. Although these harmonics are expected to occur directly from the XRES cross section,[13,21] we cannot completely rule out the contribution at $2\mathbf{q}$ arising from weak lattice modulations.[22] Using this set of four superlattice reflections, the position of the fundamental peak is refined to be $\mathbf{q}=(0,0,0.79\pm0.002)$ at this temperature. No other satellites, such as those due to the third harmonic $3\mathbf{q}$, indicative of squaring of a sinusoidal modulation, were observed in this phase.

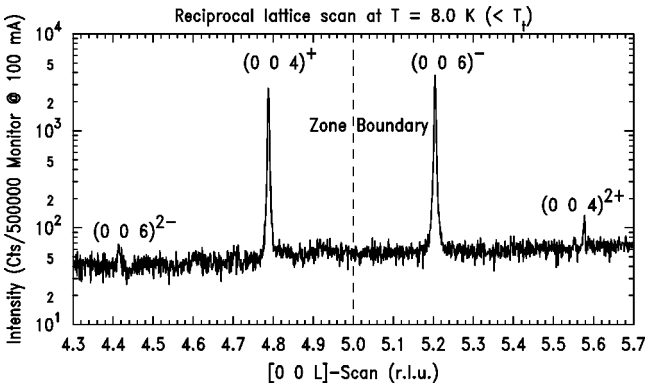

FIG. 2. Reciprocal lattice scan along $[0,0,L]$ at $T=8.0$ K taken without the analyzer. Notice that the intensity is shown on a logarithmic scale.

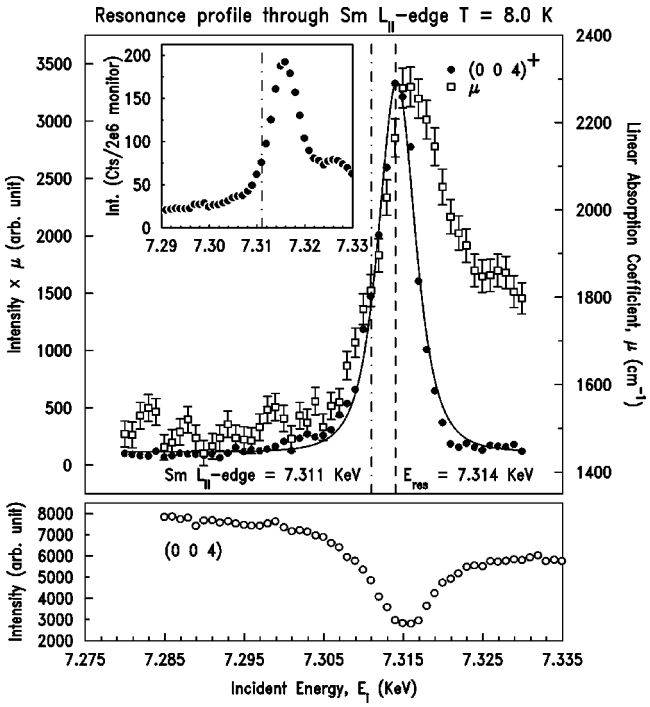

FIG. 3. Energy dependence of the superlattice peak $(0,0,4)^+$ (solid circles) through the Sm $L_{\rm II}$ edge. The data have been corrected for absorption. Open squares represent μ obtained from the fluorescence yield (see text, scale on the right). The solid line is a Lorentzian-squared fit to the elastic peak. The inset shows the energy dependence of the second harmonic (not corrected for absorption). Note the higher background (inset) above the resonance due to L_β-fluorescence contamination of the elastic channel. The dashed line locates the resonant energy, whereas the dot-dashed line indicates the absorption edge. The bottom panel shows the energy scan of the (0, 0, 4) charge Bragg peak for comparison.

Figure 3 shows an energy scan through the satellite peak at $(0,0,4)^+$. There is a strong resonance that occurs a few eV above the absorption edge, defined to be the inflection point of the fluorescence spectrum, which is consistent with the dipolar $(E1)$ nature $(2p_{1/2}\rightarrow 5d)$ and magnetic origin of the reflection. No splittings such as those measured above the $L_{\rm II}$ edge in the elemental Sm (Ref. 18) and Tb (Ref. 23) were observed. The bottom panel shows the behavior of the (0,0,4) charge peak as a function of E_i, for comparison. Although it is difficult to ascertain the true resonant enhancement relative to the nonresonant scattering, a lower limit can be estimated by simply taking the ratio of the peak to the background ~25 eV below the edge. In the present case this enhancement factor is ~35. From the fit to a Lorentzian-squared line profile, the resonant energy and width were found to be 7.314 keV and 5.4 eV (corrected for energy resolution). The width of the resonance is larger than ~4.15 eV expected from the $L_{\rm II}$ core-hole lifetime,[24] indicating that the resonance process is not dominated by the latter. A similar resonant behavior was also observed for one of the $2\mathbf{q}$ satellites (see inset of Fig. 3).

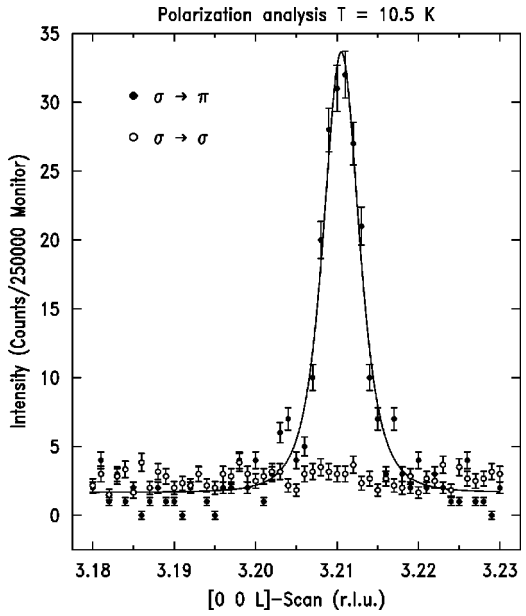

FIG. 4. Polarization analysis of the superlattice reflection, $(0,0,4)^-$. Both sets were collected on resonance using a graphite analyzer (● rotated channel, ○ unrotated channel).

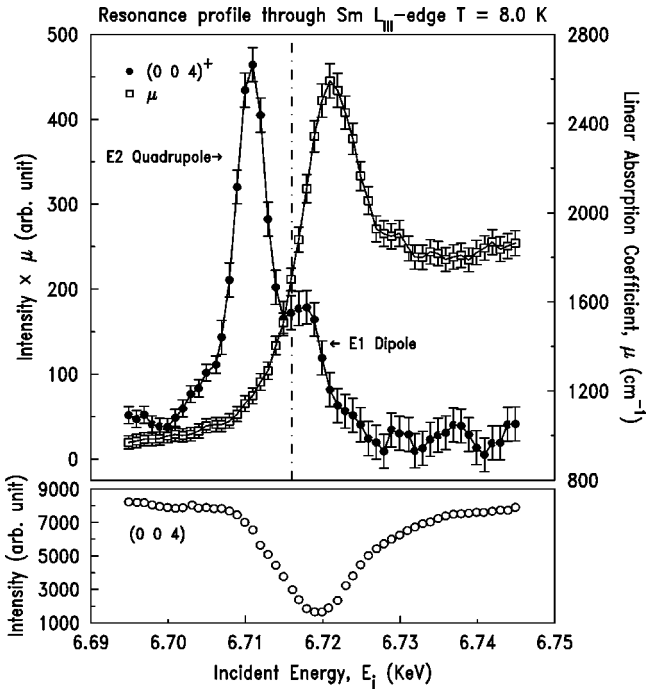

FIG. 5. Top panel: energy dependence of the magnetic peak (solid circles) through the Sm L_{III} edge, corrected for absorption. The intensities can be compared to that in Fig. 3. Open squares represent the absorption calculated using measured fluorescence spectrum (scale on the right). The solid lines are guides to the eye. The absorption edge is indicated by the vertical dot-dashed line. Bottom panel: energy scan of the (0, 0, 4) charge Bragg peak for comparison.

At 12.0 K, just above T_t but below T_N, a similar $[0,0,L]$ scan across the zone showed the same pair of magnetic satellites around the BZ boundary with a small change in their positions and diminished intensities. As in the lower-temperature phase, no third harmonics were observed. Finally, well above T_N, only charge peaks consistent with the body-centered lattice were observed, and all the magnetic peaks were absent.

Although the observation of the resonant behavior a few eV above the absorption edge, the appearance of the second harmonic, and the disappearance of the superlattice reflections above T_N are all in agreement with the magnetic nature of the superlattice peak and dipolar resonance, a critical test of the magnetic nature of the resonance is its dependence on photon polarization. In all previous XRES measurements on rare-earth nickel germanides, no polarization analyses of the resonances were performed.[25,10,11] In Fig. 4 a longitudinal scan through the superlattice peak, $(0,0,4)^-$, is displayed for $\sigma \rightarrow \pi$ and $\sigma \rightarrow \sigma$ geometries, respectively, with the E_i fixed at the resonant energy. In the case of polarization rotation, the superlattice reflection is observed, whereas in the unrotated channel the peak is barely discernible above the background. If the resonance is of magnetic character, then a complete polarization rotation should take place (see the cross section in Ref. 21), as is clearly the case.

Finally, we report the observation of a strong resonance below the Sm L_{III} edge (6.716 keV), as shown in Fig. 5, whereas no such features, except for the slight asymmetry, were detected below the L_{II} edge. The feature below the L_{II} edge is in accordance with quadrupolar ($E2$) resonance involving $2p_{3/2} \rightarrow 4f$ transition, observed in previous XRES studies on elemental Sm,[26,27] an epitaxial thin film of Sm,[18] and a $SmNi_2B_2C$ compound,[17] as well as with the resonant inelastic x-ray scattering (RIXS) on Sm.[28] Since the Coulomb interaction of the $2p$ core hole and the $4f$ electrons is stronger due to larger overlap between the two, the $E2$ resonance generally appears several eV below the $E1$ resonance. In the raw data, the $E1$ resonance was found to be significantly weaker relative to the $E2$ resonance. In order to obtain a better estimate of their relative weight, an energy scan through the edge carried out away from the magnetic peak was subtracted from the raw data, eliminating any energy dependence of the background. The data were then corrected for absorption (μ), obtained from the measured fluorescence. The edge step was normalized to the calculated μ away from the edge using tabulated values. Although this procedure does not account for the self-absorption and can introduce some systematic errors, it provides a better $E1/E2$ ratio. As the figure shows, the $E2$ resonance is significantly stronger than the $E1$ resonance and appears at 6.712 keV, ~6 eV below the latter. Similar energy scans performed at the $(0,0,4)^-$ and $(0,0,6)^{\pm}$ satellites also found the $E1$ resonance to be significantly weaker. The relative strength $I(L_{\mathrm{II}})/I(L_{\mathrm{III}})$ of the resonant enhancements (or the "branching ratio") is of interest since it relates to the underlying electronic and magnetic structures (see Refs. 15 and 29 and references therein for more details). In the present case the strength of the $E1$ resonance at L_{III} is significantly weaker than that at the L_{II} edge, with a branching ratio of ~15.

These observations can be compared to the theoretical expectations of van Veenandaal and co-workers.[29] By explicitly incorporating the expansion and contraction of the $5d$

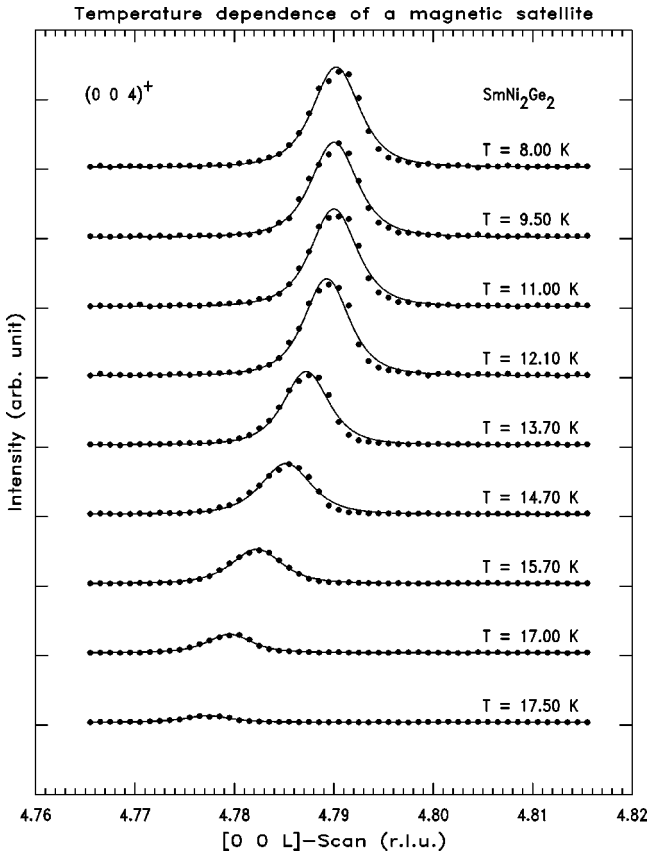

FIG. 6. Temperature dependence of the longitudinal scan through a magnetic peak. Solid lines are Lorentzian-squared fits used to extract peak positions and widths.

orbitals as was introduced by Harmon and Freeman,[30] and both spin and orbital parts of the Coulomb interaction between the localized $4f$ and the itinerant $5d$ electrons, they derived the branching ratios at the rare-earth L edges. According to their work, in light rare earths such as Sm, the $E1$ resonance at the L_{III} edge is significantly smaller than that at the L_{II} edge. Also, they showed that the quadrupolar contribution, being always relatively smaller in L_{II}, can not readily be detected due to larger lifetime broadening at this edge. Both of the above expectations are in agreement with our observations.

B. Temperature dependence

The properties of the ordered phases were measured as the temperature was raised. The measurements of the integrated intensity and the modulation vector were performed on the $(0,0,4)^{+}$ satellite. In Fig. 6 the data for the longitudinal scans through this peak are displayed. As the temperature increases, the peak intensity gradually decreases and eventually disappears above 17.8 K, consistent with the T_N obtained from $\chi(T)$. Interestingly, the position of the peak also shifts toward lower Q values as the transition is approached. Since the measurements of the (0,0,4) charge Bragg peak, as a function of temperature, found no observable expansion of the lattice, this shift in position corresponds to true changes in the magnetic modulation.

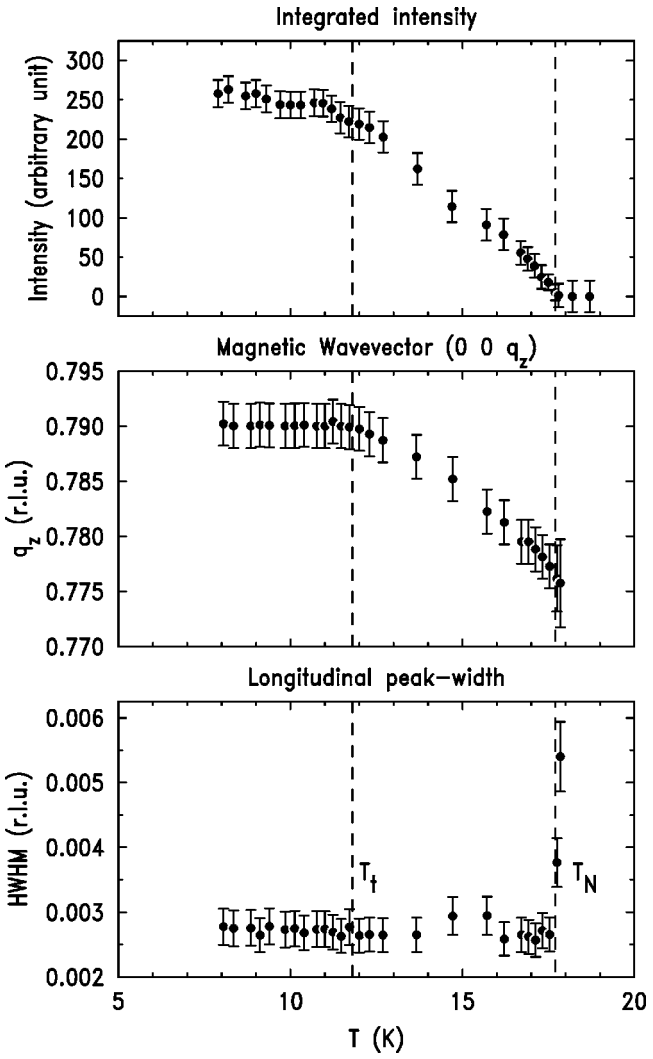

FIG. 7. Temperature dependence of the integrated intensity (top), modulation vector q_z (middle), and the longitudinal peak width (bottom).

Figure 7 summarizes the temperature dependence of the ordered phases. The integrated intensity of the magnetic peak (shown in the top panel) remains nearly temperature independent below T_t, suggesting saturation of the ordered Sm moments. Above T_t, the intensity decreases monotonically and disappears above T_N. No drastic changes in the intensity are observed as the sample passes through the transition at T_t. In comparison, the isostructural Tb (Ref. 25) and Dy (Ref. 31) nickel germanides with strong and moderate uniaxial anisotropies, respectively, the intensity displays a break at their respective T_t. In both cases, the break is associated with a transition from a amplitude-modulated (AM) phase to an equal-moment structure with maximum free-ion moment per site below T_t.

The middle panel shows the variation of the magnetic modulation with T. In the phase below T_N but above T_t, the modulation vector changes continuously with T approaching $\sim$0.775 r.l.u., indicating the incommensurate nature of the ordering, consistent with the Fermi-surface nesting picture. Below T_t, however, the structure is characterized by a

temperature-independent $\mathbf{q}=(0,0,0.79\pm0.002)$. This suggests a long-period ordered phase, in contrast to simpler commensurate AF structures found in the isostructural Tb and Dy compounds.[25,31] T_t is identified as the temperature at which **q** reaches this value with a concomitant near saturation of the intensity, which is 11.8 ± 0.2 K.

The half width at half maximum (HWHM) of the longitudinal scans is displayed in the bottom panel. The HWHM is found to be resolution limited in the entire temperature range and remains fairly constant with temperature within the experimental uncertainties. As T_N is approached from below, the HWHM sharply increases indicating a loss of magnetic correlations, consistent with a second-order-type phase transition. From the onset of broadening of the magnetic satellite T_N is inferred to be 17.7 ± 0.2 K as indicated by a vertical dashed line. We note that the reason for the small deviations of the data points near 15 K relative to the rest of the data is not clear.

C. Anisotropy of the ordered moments

The technique of using the **Q** dependence of integrated intensities of magnetic peaks in order to determine the direction of the ordered moments is rather well established. In recent years, this technique has been successfully employed in XRES studies of Gd, Nd, and Sm members of the nickel borocarbides,[32,17] and Eu, Gd, and Tb nickel germanides.[10,25] The details of the measurement technique and modeling can be found in Refs. 33, 21, and 11. Figure 8 shows the **Q** dependence of the integrated intensities of the magnetic peaks measured on resonance at $E_i=7.314$ keV. At 8.0 K, the measurements were repeated 3 times, in symmetric reflection geometry, in order to assess the errors and reproducibility of the data. The measured intensities were found to be within the error bars displayed in the figure. A geometric correction to the two low-Q data points has been applied to reduce systematic errors, which are severe at small angles, due to surface miscut.[34]

In order to explain the behavior of the **Q** dependence we carried out model calculations based upon the resonant cross section. In the case of dipolar resonance the intensity of the first-order magnetic satellite for linearly polarized incident x rays is given by[21]

$$I(\mathbf{Q})=C\sum_{\text{domain}}\left|\left(\sum_n \hat{\mathbf{k}}'\cdot\hat{\mathbf{z}}_n\right)\right|^2,$$

where C includes a **Q**-independent resonant amplitude and geometric and arbitrary scale factors, $\hat{\mathbf{k}}'$ is the direction of the scattered beam, $\hat{\mathbf{z}}_n$ is the moment direction at site n, and a summation over the symmetry-equivalent domains is also carried out. At resonance, nonresonant contributions are small and can be neglected. Note that only the components of the moments in the scattering plane contribute to the cross section. So the case of a basal-plane helical structure is indistinguishable from a plane wave with the moments pinned along some crystallographic axis within the basal plane. In addition, the absolute magnitude of the moments cannot be determined using this technique.

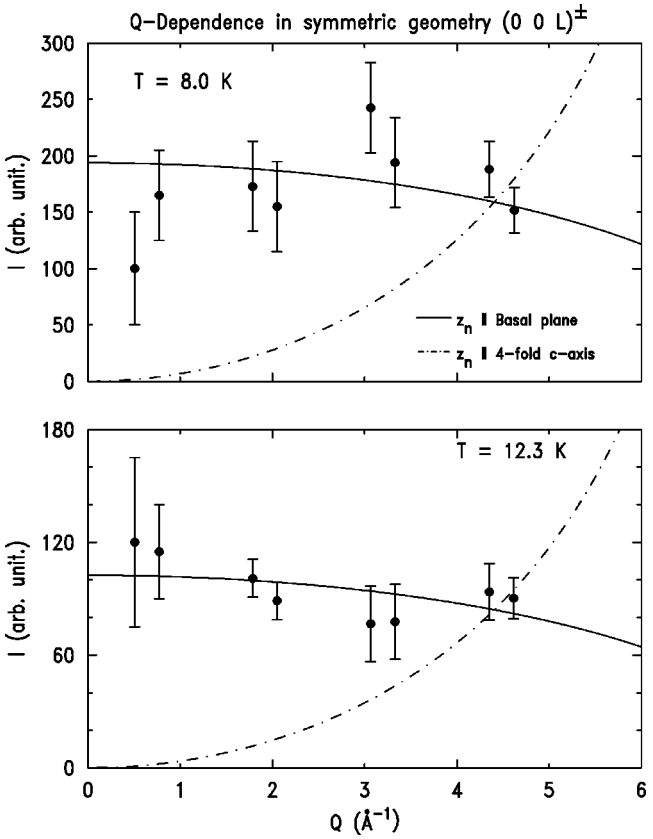

FIG. 8. The **Q** dependence of integrated intensities of magnetic peaks. The solid line is for a model with the ordered moments $\perp\hat{\mathbf{c}}$ and the dashed line is for that with moments $\parallel\hat{\mathbf{c}}$.

Two models, a basal-plane helix ($\hat{\mathbf{z}}_n\perp\hat{\mathbf{c}}$) and a longitudinal spin wave ($\hat{\mathbf{z}}_n\parallel\hat{\mathbf{c}}$), respectively, were considered. As can be seen in Fig. 8, in both phases the data (solid circles) can be modeled well with the ordered moments in the basal plane (solid line). Similar trends in the **Q** dependence were observed for Eu and Gd nickel germanides[10] in their low-temperature phases with the moments locked in the basal plane. On the other hand, the model with the moments along the $\hat{\mathbf{c}}$ axis is manifestly in disagreement with the data. This behavior is consistent with the anisotropy observed in the susceptibility measurements[12] summarized above. Given the experimental errors, the direction of the ordered moments is determined within $\sim10°$ of the basal plane.

IV. CONCLUSIONS

In summary, using the XRES technique, we have shown that the magnetic structures of the neutron-opaque Sm member of the $R\mathrm{Ni}_2\mathrm{Ge}_2$ series conform to the topological nesting of the Fermi surface. $\mathrm{SmNi}_2\mathrm{Ge}_2$ orders in an *incommensurate* AF structure characterized by a single propagation vector $\mathbf{q}=(0,0,q_z)$. The value of q_z is T dependent and approaches ~0.775 r.l.u. near $T_N=17.7\pm0.2$ K. Below T_t, the ordered moments saturate and the modulation vector attains a T-independent value of $(0,0,0.79\pm0.002)$. No evidence of a squaring-up of this structure was observed. In both the

ordered phases the ordered moments are confined to the basal plane.

As mentioned above, due to the fourfold symmetry of the basal plane it is not possible to distinguish a plane wave with moments locked in along, for example, $\hat{\mathbf{a}}$ (or $\hat{\mathbf{b}}$), from a basal-plane helix. A preferred direction within the plane near T_N is unlikely, however, since the higher-order CEF terms are relatively weak according to the Zener power law. So we can state that the phase above T_t is most likely a basal-plane helix. At lower T, as the system becomes more ordered, higher-order CEF terms become significantly important, which can lead to a directional lock-in transition.

The behavior of $\mathbf{q}$ as a function of temperature may be explained, qualitatively, according to the theoretical work of Elliot and Wedgewood.[35,36] In this theory, as the magnetic order develops, the conduction electrons experience a new translational symmetry associated with the periodic exchange field, which introduces new superzone boundaries. As a result, new gaps appear in the energy bands at these boundaries, and the Fermi level shifts with the growth of the ordered moments. This dependence of the gap and the shift of the Fermi level on the ordered moment leads to a variation of $\mathbf{q}$ with T. As the moments saturate, $\mathbf{q}$ becomes T independent as well. This situation prevails as long as the relative stability of a magnetic structure with a given $\mathbf{q}$ at a particular temperature is determined by internal energy (U) alone. As pointed out by Cooper,[4] for a magnetic spiral with the same ordered moment per R ion, the entropy (S) considerations can be neglected and $\mathbf{q}$ attains the value that minimizes the exchange energy at a given T. This behavior is in stark contrast to the c-axis modulated (CAM) phase, such as that found in $TbNi_2Ge_2$ compound, where entropy plays a critical role in stabilizing the amplitude-modulated structure near T_N.[37,3] Below $T_t \sim \frac{1}{2} T_N$, the CAM phase lowers the free energy ($F=U-TS$) by developing higher harmonics, which leads to squaring up of the structure with the free-ion value for the moment per site.

The behavior of the HWHM through T_t also contrasts with that observed in the isostructural Tb compound.[25] In $TbNi_2Ge_2$, the HWHM broadens beyond instrumental resolution below T_t, indicating a reduction of the magnetic correlation length (ξ_m) in the phase below this transition. The reduction of ξ_m was ascribed to the formation of small antiphase domains separated by AF planes, as the incommensurate CAM phase squares up into a commensurate structure characterized by $(\frac{3}{4},0,0)$ below T_t. In the case of the $SmNi_2Ge_2$, no such broadening below T_t of the HWHM beyond the resolution was observed suggesting the absence of such antiphase-domain formation.

It is interesting to note that the modulation vector $\mathbf{q}=(0,0,0.79)$ characterizing the ground state is not unique to the Sm member of the series. $GdNi_2Ge_2$, for instance, also orders at this same $\mathbf{q}$ value near T_N, as well as one of the more stable low-T metamagnetic phases of $TbNi_2Ge_2$.[11] This tendency ties in well with the calculations of $\chi_0(\mathbf{q})$, which exhibits a pronounced maximum at this wave vector corresponding to a strong nesting of the Fermi surface.[10,11]

Finally, in addition to studying the magnetic structures, we observed a clear quadrupolar resonance below the Sm L_{III} edge, significantly stronger than the dipolar resonance above this edge. Also, the branching ratio for the dipolar resonances was found to be ~ 15, the resonance at the L_{II} being higher. These results are consistent with the theoretical framework proposed by van Veenendaal and co-workers,[29] as discussed above.

ACKNOWLEDGMENTS

We would like to thank J. Pollmann for his help during the initial set up of the experiment, as well as D. Haskel, D. Wermeille, and S. K. Sinha for stimulating discussions on rare-earth magnetism, magnetic resonance, and related phenomena. A.P.S. is supported by the U.S. DOE, Office of Science, under Contract No. W-31-109-ENG-38. Part of this work is supported by the State of Illinois under HECA. Ames Laboratory (DOE) is operated by Iowa State University under Contract No. W-7405-Eng-82.

*Electronic address: zahir@aps.anl.gov

[1] A. Szytula and J. Leciejewicz, *Handbook of Crystal Structures and Magnetic Properties of Rare Earth Intermetallics* (CRC Press, Boca Raton, 1994), pp. 114–192.

[2] D. Gignoux and D. Schmitt, *Handbook of Magnetic Materials* (Elsevier, Amsterdam, 1997), pp. 239–413.

[3] R. J. Elliot, in *Magnetism*, edited by G. T. Rado and H. Suhl (Academic, New York, 1965), Vol. IIA, p. 385.

[4] B. R. Cooper, in *Solid State Physics*, edited by F. Seitz, D. Turnbull, and H. Ehrenreich (Academic, New York, 1968), Vol. 21, p. 393.

[5] S. Liu, in *Handbook on the Physics and Chemistry of Rare Earths*, edited by K. A. Gschneidner, Jr. and L. Eyring (North-Holland, Amsterdam, 1978), Vol. 1, p. 233.

[6] W. Rieger and E. Parthé, Monatsch. Chem. **100**, 444 (1969); H. Pinto, M. Melamud, M. Kuznietz, and H. Shaked, Phys. Rev. B **31**, 508 (1985); A. Szytula, A. Oleś, Y. Allain, and G. Andreé, J. Magn. Magn. Mater. **75**, 298 (1988); J. K. Yakinthos, *ibid.* **99**, 1123 (1991); G. Andŕe, P. Bonville, F. Bourée, A. Bombik, M. Kolenda, A. Oleś, A. Pacyna, W. Sikora, and A. Szytula, J. Alloys Compd. **224**, 253 (1995).

[7] J. Jensen and A. R. Mackintosh, *Rare Earth Magnetism* (Oxford University Press, New York, 1991).

[8] S. K. Sinha, in *Handbook on the Physics and Chemistry of Rare Earths*, edited by K. A. Gschneidner, Jr. and L. Eyring (North-Holland, Amsterdam, 1978), Vol. 1, p. 489.

[9] L. M. Roth, H. J. Zeiger, and T. A. Kaplan, Phys. Rev. **149**, B519 (1966).

[10] Z. Islam, C. Detlefs, C. Song, A. I. Goldman, V. Antropov, B. N. Harmon, S. L. Bud'ko, T. Wiener, P. C. Canfield, D. Wermeille, and K. D. Finkelstein, Phys. Rev. Lett. **83**, 2817 (1999).

[11] Z. Islam, Ph.D. thesis, Iowa State University, 1999.

[12] S. L. Bud'ko, Z. Islam, T. A. Wiener, I. R. Fisher, A. H. Lacerda, and P. C. Canfield, J. Magn. Magn. Mater. **205**, 53 (1999).

[13] J. P. Hannon, G. T. Trammell, M. Blume, and D. Gibbs, Phys. Rev. Lett. **61**, 1245 (1988).

[14] D. Gibbs, D. R. Harshman, E. D. Isaacs, D. B. McWhan, D. Mills, and C. Vettier, Phys. Rev. Lett. **61**, 1241 (1988).

[15] D. F. McMorrow, D. Gibbs, and J. Bohr, in *Handbook on the Physics and Chemistry of Rare Earths*, edited by K. A. Gschneidner, Jr. and L. Eyring (North-Holland, Amsterdam, 1997), Vol. 26, p. 1; D. Gibbs, J. P. Hill, and C. Vettier (unpublished).

[16] D. B. McWhan, J. Synchrotron Radiat. **1**, 83 (1994).

[17] C. Detlefs, A. H. M. Z. Islam, A. I. Goldman, C. Stassis, P. C. Canfield, J. P. Hill, and D. Gibbs, Phys. Rev. B **55**, R680 (1997).

[18] A. Stunault, C. Vettier, N. Bernhoeft, F. de Bergevin, C. Dufour, and K. Dumesnil, Proc. SPIE **3773**, 295 (1999).

[19] P. C. Canfield and Z. Fisk, Philos. Mag. B **56**, 1117 (1992).

[20] J. C. Lang, G. Srajer, J. Wang, and P. L. Lee, Rev. Sci. Instrum. **70**, 4457 (1999).

[21] J. P. Hill and D. F. McMorrow, Acta Crystallogr., Sect. A: Found. Crystallogr. **5**, 236 (1996).

[22] J. Bohr, D. Gibbs, D. E. Moncton, and K. L. D'Amico, Physica A **140**, 349 (1986).

[23] S. C. Perry, M. M. R. Costa, W. G. Stirling, M. J. Longfield, D. Mannix, and T. Brückel, J. Phys.: Condens. Matter **10**, 1951 (1998).

[24] M. D. Hamrick, Master's thesis, Rice University, 1990.

[25] Z. Islam, C. Detlefs, A. I. Goldman, S. L. Bud'ko, P. C. Canfield, J. P. Hill, D. Gibbs, T. Vogt, and A. Zheludev, Phys. Rev. B **58**, 8522 (1998).

[26] D. Watson, E. M. Forgan, W. G. Stirling, W. J. Nuttall, S. C. Perry, M. M. R. Costa, and D. Fort, J. Magn. Magn. Mater. **140–144**, 743 (1995).

[27] S. L. Lee, E. M. Forgan, S. J. Shaikh, C. C. Tang, W. G. Stirling, S. Langridge, A. J. Rollason, M. M. R. Costa, M. J. Cooper, E. Zukowski, J. B. Forsyth, and D. Fort, J. Magn. Magn. Mater. **127**, 145 (1993).

[28] J.-J. Gallet, J.-M. Mariot, L. Journel, C. F. Hague, A. Rogalev, H. Ogasawara, A. Kotani, and M. Sacchi, Phys. Rev. B **60**, 14 128 (1999).

[29] M. van Veenendaal, J. B. Goedkoop, and B. T. Thole, Phys. Rev. Lett. **78**, 1162 (1997).

[30] B. N. Harmon and A. J. Freeman, Phys. Rev. B **10**, 1979 (1974).

[31] Z. Islam, C. Detlefs, A. I. Goldman, S. L. Bud'ko, P. C. Canfield, and A. Zheludev, Solid State Commun. **108**, 371 (1998).

[32] C. Detlefs, A. I. Goldman, C. Stassis, P. C. Canfield, B. K. Cho, J. P. Hill, and D. Gibbs, Phys. Rev. B **53**, 6355 (1996).

[33] C. Detlefs, Ph.D. thesis, Iowa State University, 1999.

[34] The pair of lowest-Q data points were severely attenuated due to large reduction of scattering volumes since the Bragg angles for these reflections $\sim$3.9° and $\sim$5.9°, respectively, were very close to the miscut angle estimated to be 3.5°. Similar systematic reductions have also been observed in earlier measurements on $GdNi_2B_2C$ (Ref. 32) and $TbNi_2Ge_2$ (Ref. 25). In both of these cases the samples were cut and polished by conventional means. In contrast, no such systematic reductions of the intensities were observed in $EuNi_2Ge_2$ compound where an as-grown surface was used (Ref. 10). A simple geometric correction was applied to the two low-Q data points, noting that detected scattered photons come from within one absorption length of the exit face. In the present case this amounts to a reduction of factors of $\sim$15 and $\sim$5, respectively, for the lowest-Q data points compared to the case with no asymmetry.

[35] R. J. Elliot and F. A. Wedgewood, Proc. Phys. Soc. London **84**, 63 (1964).

[36] R. J. Elliot and F. A. Wedgewood, Proc. Phys. Soc. London **81**, 846 (1963).

[37] R. J. Elliot, Phys. Rev. **124**, 346 (1961).